Transition-metal Complexes of Pyrrole Pigments. XIX. Electrochemical and Coordination Behaviors of (5,10,15,20-Tetraphenylporphinato)niobium(V) Complexes†

Yoshihisa MATSUDA, Sunao YAMADA, Takashi GOTO, and Yukito MURAKAMI*

Department of Organic Synthesis, Faculty of Engineering, Kyushu University, Hakozaki, Higashi-ku, Fukuoka 812

(Received July 11, 1980)

The redox chemistry of acetato(5,10,15,20-tetraphenylporphinato)oxoniobium(V) (**1**) was investigated in dichloromethane by means of cyclic voltammetry and controlled potential electrolysis. One-electron reduction potentials were observed at −0.89, −1.05, and −1.41 V *vs.* SCE for the range from 0 to −2.0 V; the reduction of niobium(V) to niobium(III) occurred prior to ligand-reduction. The potential separation between first and second metal-reductions ($\Delta E_{1/2}$) for **1** is 0.16 V, while $\Delta E_{1/2}$ between reductions of the Mo^{VI} and Mo^{V} species for the corresponding molybdenum complex is 1.24 V. In order to elucidate the origin of such potential difference between the niobium and molybdenum complexes, the change of coordination structures which takes place in the course of redox reactions was examined. The coordination reaction of **1** with pyridine was also studied.

As a step toward preparation of one-dimensional electric conductors by stacking planar complexes with the formation of metal–metal bonds, molybdenum and niobium complexes of macrocyclic tetrapyrroles are plausible ones for this purpose since the metal ions have a strong tendency to form metal to metal bonds in their low oxidation states. The redox behaviors of these metal complexes needs to be investigated in order to establish chemical conditions for the formation of complexes involving low valency metals. We have previously studied the redox properties of several molybdenum(V) complexes of macrocyclic tetrapyrroles.[1] Acetato(5,10,15,20-tetraphenylporphinato)oxoniobium(V) [Nb^{V}(O)(TPP)(AcO), **1**][2] and tri-μ-oxo-bis[(5,10,15,20-tetraphenylporphinato)niobium(V)] [$Nb^{V}_2(O)_3(TPP)_2$, **2**][3,4] have been prepared and their crystallographic structures determined. However, the redox chemistry of these niobium complexes has not been examined so far.

We have investigated in the present work the redox properties of Nb^{V}(O)(TPP)(AcO) by cyclic voltammetry and controlled potential electrolysis in reference to the behavior of the corresponding molybdenum(V) complex, Mo^{V}(O)(TPP)(AcO), and the niobium(III) species was produced electrochemically for the first time. Since Nb^{V}(O)(TPP)(AcO) and $Nb^{V}_2(O)_3(TPP)_2$ assume a unique hepta-coordination geometry around the niobium(V) atom, the coordination interactions of both complexes with pyridine as well as the interaction of the latter complex with acetic acid have also been studied.

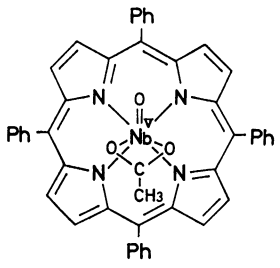

Nb(O)(TPP)(AcO)

† Contribution No. 596 from this Department.

Experimental

Materials. Acetato(5,10,15,20-tetraphenylporphinato)-oxoniobium(V) [Nb^{V}(O)(TPP)(AcO), **1**] and tri-μ-oxo-bis[(5,10,15,20-tetraphenylporphinato)niobium(V)] [$Nb^{V}_2(O)_3(TPP)_2$, **2**] were prepared by the methods of Lecomte and Protas.[2] Dichloromethane was treated with concentrated sulfuric acid, neutralized with aqueous sodium hydroxide, washed with distilled water, and refluxed over anhydrous calcium chloride for 2 d. After being fractionally distilled, dichloromethane thus purified and dried was stored over molecular sieve (3A, 1/16; Ishizu Pharmaceutical Co.). Pyridine was refluxed over potassium hydroxide and fractionally distilled. Tetrabutylammonium perchlorate (TBAP) of polarographic grade (Nakarai Chemicals) was used without further purification.

Spectroscopic Measurements. A Bruker WH-90 FT and a Hitachi R-24B spectrometer were used to obtain ^{1}H NMR spectra in chloroform-*d* (>99.5%; E. Merck, Darmstadt) at room temperature. Chemical shifts are given in ppm from internal TMS and calibrated with a chloroform signal as the secondary external reference. ESR spectra were recorded on a JEOL JES-ME-3 X-band spectrometer equipped with a 100 kHz field modulation unit; a standard MgO/Mn(II) sample calibrated with a NMR magnetometer was employed for calibration of the magnetic field. Electronic spectra were taken on a Union Giken SM-401 high sensitive spectrophotometer at 25 °C.

Electrochemical Measurements. Cyclic voltammetry was carried out on a YANACO P-8 polarograph equipped with platinum wire of 0.5 mm diameter as working and auxiliary electrodes; the surface area of the former electrode being about 30 times smaller than that of the latter. A saturated calomel electrode (SCE) was served as a reference which was separated from a bulk electrolyte solution by a salt bridge prepared with benzyliden-D-glucitols[5] and a dichloromethane solution of TBAP. A dichloromethane solution containing a niobium complex (5.0×10^{-4} mol dm^{-3}) and TBAP (5.0×10^{-2} mol dm^{-3}) was deaerated prior to each measurement and the inside of the cell was maintained under argon atmosphere throughout each measurement. All the measurements were carried out at 25±2 °C. The scan rate was varied in a range from 5 to 500 mV s^{-1}. Half-wave potentials ($E_{1/2}$) and anodic (i_{pa}) and cathodic (i_{pc}) currents were evaluated by referring to the literature methods.[6]

Controlled potential electrolysis was carried out in a three-electrode cell, modified for ESR and electronic spectral

measurements, with platinum wire of 0.5 mm diameter as working and auxiliary electrodes. The reference electrode was the same as used for cyclic voltammetry. An applied potential between the working and auxiliary electrodes was maintained constant with a conventional potentiostat and monitored with a Takeda Riken TR-6656 digital multimeter.

Results

Coordination Behavior of Nb(O)(TPP)(AcO). In order to examine the further coordination ability of **1**, the interaction between **1** and pyridine was investigated by electronic and NMR spectroscopy. The electronic spectrum of **1** was measured by changing the concentration of pyridine in a range of 0 to 3.09 mol dm^{-3} while the concentration of **1** was maintained constant (3.7×10^{-6} mol dm^{-3}). The results are shown in Fig. 1, where

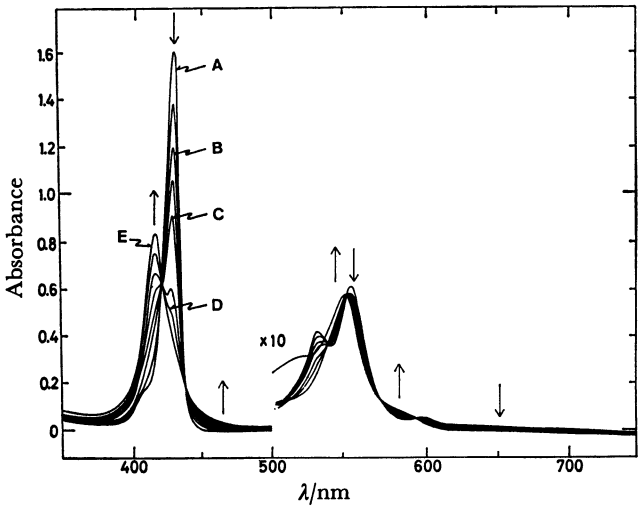

Fig. 1. Electronic spectra of Nb(O)(TPP)(AcO) (3.7×10^{-6} mol dm^{-3}) at 25.2 °C in the presence of pyridine at various concentrations (0—3.09 mol dm^{-3}): A, 0; B, 3.09×10^{-2}; C, 1.55×10^{-1}; D, 6.18×10^{-1}; E, 3.09 mol dm^{-3}. Trends of spectral change with increase in pyridine concentration are shown by arrows (↑ and ↓).

isosbestic points are observed at 420, 437, ≈510, 538, 550, 575, and 593 nm. The spectral behavior shows the formation of a single pyridine adduct of **1**. The NMR spectra clearly indicate the coordination of pyridine to **1**. A methyl signal of the coordinated acetate for **1** was observed at 1.27 ppm as shown in Fig. 2; appeared in a upper field range relative to the signal of acetic acid (2.20 ppm). This is attributed to a magnetic anisotropy effect provided by the macrocyclic ligand on the coordinated acetate group. This signal was, however, drastically shifted to a lower field range (5.28 ppm) in chloroform–pyridine (7 : 3 v/v) as shown in Fig. 2. This indicates that the methyl protons are displaced from a shielding to a deshielding zone of the porphyrin skeleton. Furthermore, signals due to the coordinated pyridine were observed in a range of 6 to 7 ppm, which are separated from those of the coordination-free pyridine appeared in the lower field range. By referring to the signal intensity of methyl protons

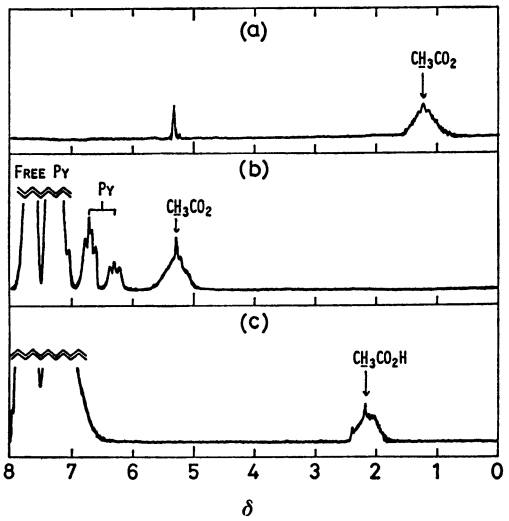

Fig. 2. NMR spectra of Nb(O)(TPP)(AcO) and acetic acid at room temperature: (a), Nb(O)(TPP)(AcO) in chloroform-*d* (a signal due to dichloromethane used as solvent for recrystallization appeared at 5.31 ppm); (b), Nb(O)(TPP)(AcO) in pyridine–chloroform-*d* (3 : 7 v/v); (c), acetic acid in pyridine–chloroform-*d* (3 : 7 v/v).

of the coordinated acetate, a number of pyridine molecules coordinated to **1** was evaluated to be one. Other signals observed in a low-field region below 7 ppm are: 7.78 (12H, m, *m*- and *p*-phenyl H's), 8.22 (8H, m, *o*-phenyl H's), and 9.04 (8H, s, pyrrole H's). The effect of pyridine coordination on the electronic and NMR spectra is consistent with the following solution equilibrium, where Py stands for pyridine.

$$\text{Nb(O)(TPP)(AcO)} + \text{Py} \overset{K}{\rightleftharpoons} \text{Nb(O)(TPP)(AcO)(Py)} \qquad (1)$$

The equilibrium constant (K) was obtained from the intensity change at 427 nm by the aid of Benesi-Hildebrand equation[7] (Eq. 2), where $[Nb]_T$ and $[Py]_T$ stand for the total concentrations of **1** and pyridine, respectively; $\Delta\varepsilon$ is for the difference in molar absorption coefficient between **1** and its pyridine adduct, and ΔA represents the extent of absorbance change upon

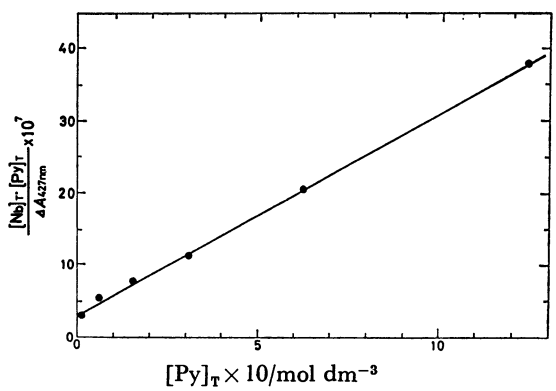

Fig. 3. Benesi-Hildebrand plot for the complex-forming equilibrium between Nb(O)(TPP)(AcO) and pyridine.

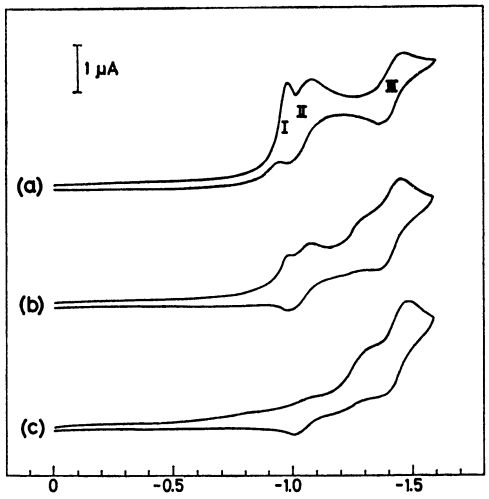

Fig. 4. Cyclic voltammograms of Nb(O)(TPP)(AcO) (5.0×10^{-4} mol dm^{-3}) in dichloromethane containing TBAP (5.0×10^{-2} mol dm^{-3}) at 25.2 °C in the presence of pyridine at various concentrations: (a), 0; (b), 0.8; (c), 3.5 mol dm^{-3}; scan rate 50 mV s^{-1}.

addition of pyridine. A good linear correlation based

$$\frac{[\mathrm{Nb}]_\mathrm{T}[\mathrm{Py}]_\mathrm{T}}{\Delta A}=\frac{1}{\Delta\varepsilon\cdot K}+\frac{[\mathrm{Py}]_\mathrm{T}}{\Delta\varepsilon} \quad (2)$$

on Eq. 2 is observed as shown in Fig. 3: $K=9.6$ mol^{-1} dm^3; and $\Delta\varepsilon=3.48\times10^5$. The $\Delta\varepsilon$-value is in good agreement with that observed in the presence of a large excess of pyridine (3.44×10^5). The coordination of pyridine to **1** was also confirmed by cyclic voltammetry as shown in Fig. 4. Addition of pyridine to **1** resulted in marked cathodic shifts of reduction peaks I and II, from *ca.* −1 to −1.3 V *vs.* SCE, and the corresponding oxidation peaks appeared at −1.2 and −1.0 V *vs.* SCE. Redox peaks III, however, remained almost unchanged even in the presence of a large excess of pyridine.

Interaction of $Nb_2(O)_3(TPP)_2$ with Acetic Acid. The cyclic voltammogram of **2** for the range of 0 to −2.0 V *vs.* SCE in dichloromethane is shown in Fig. 5. The distinct cathodic peaks at −1.30, −1.56, and −1.80 V are coupled with anodic peaks at −1.23, −1.44, and −1.66 V, respectively, each being referred to one-electron transfer process. Redox peaks due to **1** appeared upon addition of acetic acid to a solution of **2**, and the cyclic voltammogram was completely converted to that of **1** in the presence of a 2-fold excess amount of acetic acid as shown in Fig. 5. Such conversion of **2** into **1** through reaction with acetic acid was also confirmed by electronic spectroscopy. The spectral change upon addition of acetic acid to **2** is shown in Fig. 6, where isosbestic points are observed at 421, 441, ≈500, 540, and 551 nm. Since the reaction was accelerated under anaerobic conditions, oxygen must participate in the reverse reaction as shown by Eq. 3.

$$\mathrm{Nb_2(O)_3(TPP)_2}+2\mathrm{AcOH}\underset{\mathrm{O_2}}{\rightleftharpoons}2\,\mathrm{Nb(O)(TPP)(AcO)}+\mathrm{H_2O} \quad (3)$$

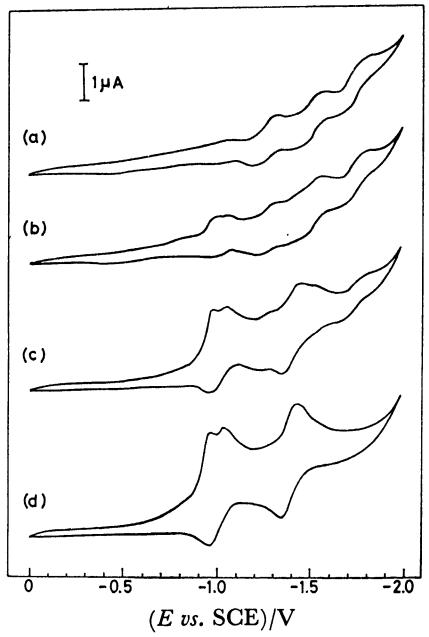

Fig. 5. Cylic voltammograms of $Nb_2(O)_3(TPP)_2$ (2.4×10^{-4} mol dm^{-3}) in dichloromethane containing TBAP (5.0×10^{-2} mol dm^{-3}) at 24 °C in the presence of acetic acid at various concentrations: (a), 0; (b), 1.24×10^{-4}; (c), 4.7×10^{-4}; (d), 9.7×10^{-4} mol dm^{-3}; scan rate 100 mV s^{-1}.

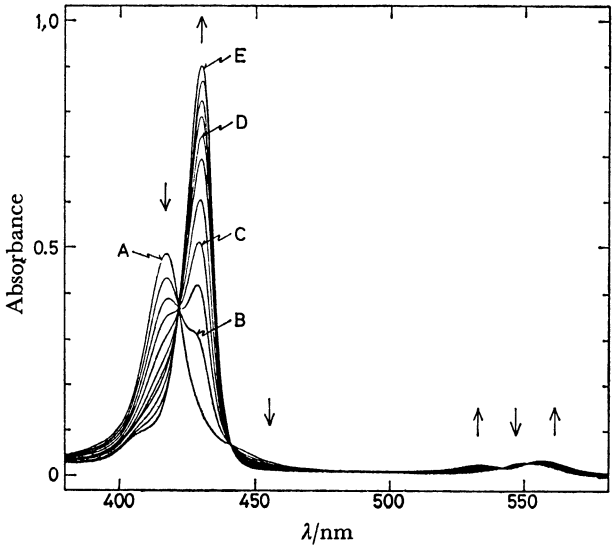

Fig. 6. Electronic spectral change during the reaction of $Nb_2(O)_3(TPP)_2$ (2.3×10^{-6} mol dm^{-3}) with acetic acid (7.1×10^{-5} mol dm^{-3}) in dichloromethane at 25 °C: A, 0; B, 0.5; C, 1.5; D, 3.0; E, 7.5 h. Trends of spectral change with time are shown by arrows (↑ and ↓).

Electrochemical Behavior of Nb(O)(TPP)(AcO). A typical cyclic voltammogram of **1** for the range of 0 to −1.6 V *vs.* SCE in dichloromethane is shown in Fig. 4. No other peak was observed in a cathodic range up to −2.0 V at any scan rate in a range from 10 to 200 mV s^{-1}. Two distinct cathodic peaks at −1.09 and −1.47 V are coupled with anodic peaks at −0.98 and −1.36 V, respectively. Although the anodic wave

coupled with the first cathodic peak at −0.97 V *vs.* SCE was obscure for faster scan rates, it became apparent by reducing the rate below 20 mV s^{-1}. We, therefore, evaluated three half-wave potentials for one-electron reduction steps, indicated by I, II, and III in Fig. 4(a), as −0.89, −1.05, and −1.41 V *vs.* SCE (within an accuracy of ±0.02 V), respectively. It has been generally realized that redox potentials of the central metal atom, incorporated into planar complexes formed with macrocyclic ligands, are quite sensitive to the nature of axial ligands, while those of the macrocyclic ligands are hardly affected by the variation of such ligands.[8] In the light of the coordination effect provided by pyridine on redox potentials, as described in a foregoing section, peaks I and II in Fig. 4(a) are attributed to the reductions of niobium, Nb^{V}/Nb^{IV} and Nb^{IV}/Nb^{III}, respectively, and peak III is due to that of the porphyrin ligand.

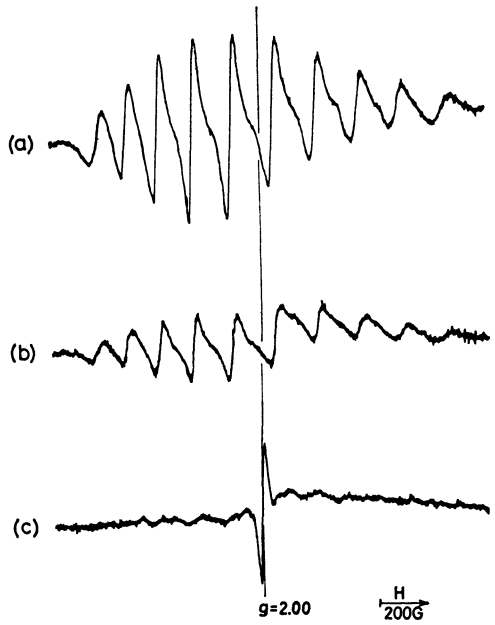

Fig. 7. ESR spectral change during the electrochemical reduction of Nb(O)(TPP)(AcO) at room temperature in dichloromethane containing TBAP (0.30 mol dm^{-3}) at potentials: (a), −0.92; (b), −1.1; (c), −1.46 V *vs.* SCE

We carried out the controlled potential reduction of **1** at −0.92, −1.1, and −1.46 V *vs.* SCE in dichloromethane in the presence of TBAP; potentials sufficient for respective one-electron reductions of **1** as confirmed by voltammetric measurements. The parent complex is diamagnetic itself, so that no ESR signal was observed. When **1** was reduced at −0.92 V *vs.* SCE, ten intense lines caused through interaction with ^{93}Nb (I=9/2) nucleus were observed over a wide range of magnetic field as shown in Fig. 7(a); this indicates the formation of a paramagnetic niobium(IV) species. These lines, however, decreased their intensities to a large extent upon electrolysis at −1.1 V *vs.* SCE as shown in Fig. 7(b). This implies that the two-electron reduced species is either a diamagnetic niobium(III) complex or a paramagnetic spin-triplet species involving unpaired electrons in both metal and ligand sites, such as π-cation radical of copper(II)–porphyrin.[9] A considerable cathodic shift of peak II upon addition of pyridine to **1** as demonstrated by cyclic voltammetry as well as the ESR pattern for a species obtained by the following electrolysis at peak III range excludes the latter possibility. The controlled potential reduction at −1.46 V *vs.* SCE provided a new signal due to a radical species with concomitant disappearance of the lines due to ^{93}Nb nucleus as shown in Fig. 7(c). The third reduction step undoubtedly corresponds to reduction of the porphyrin ligand. Reversible oxidation reactions were observed after ceasing the respective electrolytic reductions. As a result, complete redox behavior of **1** is illustrated as in Scheme 1.

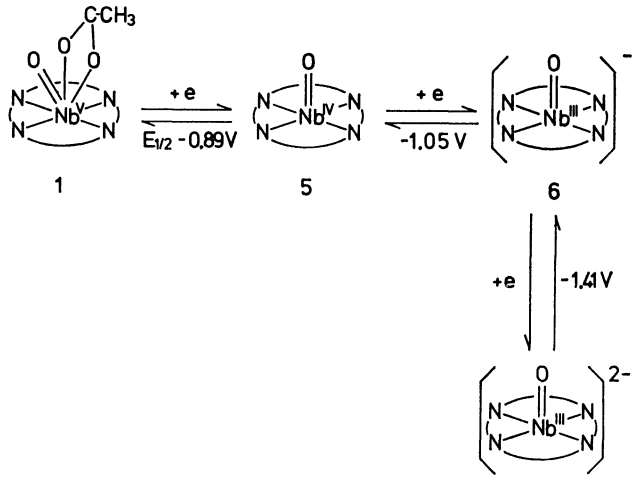

Scheme 1.

Discussion

The tri-μ-oxo dimer (**2**) does not undergo coordination interaction with pyridine as confirmed by cyclic voltammetry. An overall feature as well as cathodic and anodic peak potentials of the voltammogram was not influenced by the presence of pyridine for its concentration range from 0 to 3.5 mol dm^{-3} under otherwise identical conditions as stated in Fig. 5. According to the X-ray crystallographic analysis of **2**,[3,4] each niobium atom is hepta-coordinate and displaced from the mean ligand plane toward the tri-μ-oxo group by 1.01 Å as shown in **3**. Thus, an additional ligand can not attack at the axial site *trans* to the tri-μ-oxo group due to geometrical reasons, and must approach from the site sandwiched in between the two porphyrin ligands. As a result, pyridine fails to interact with niobium(V) likely due to steric hindrance while acetic acid undergoes substitution reaction with **2** to yield **1**. The coordination geometry around niobium(V) for **1** bears a close

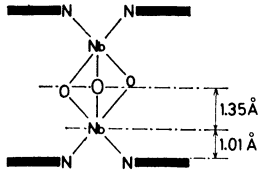

3

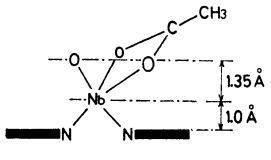

4

Table 1. Reduction and oxidation potentials for H_2TPP and its niobium and molybdenum complexes in dichloromethane at 25 °C in the presence of TBAP (5.0×10^{-2} mol dm^{-3})[a]

Compound	Metal			Ligand		Reference
	$E^{ox}_{1/2}$	$E^{red}_{1/2}(1)$	$E^{red}_{1/2}(2)$	$E^{red}_{1/2}(1)$	$E^{red}_{1/2}(2)$	
H_2TPP				−1.23	−1.56	1
				−1.21		13
Nb(O)(TPP)(AcO)		−0.89	−1.05	−1.41	[c]	This work
Mo(O)(TPP)(AcO)[b]	1.2	−0.04		−1.11	−1.51	1

a) $E_{1/2}$ values are given in V *vs.* SCE; within an accuracy of ±0.02 V. b) Acetic acid (1.0 mol dm^{-3}) added. c) No peak was detected in a cathodic range up to −2.0 V.

Table 2. Physical parameters for niobium(IV) and molybdenum(V) complexes

Complex	$\nu_{M=O}$/cm^{-1} [a]	Spin Hamiltonian parameters[b]			$\lvert\mu_I\rvert$[c]	$\rho\times10^4$ [d]
		g	$A_{metal}\times10^4$/cm^{-1}	$A_N\times10^4$/cm^{-1}		
Nb^{IV}(O)(TPP)[e]	(905)[f]	1.96	175	—	6.17	127.8
Mo^{V}(O)(TPP)(AcO)[g]	942, 919	1.961	48.5	2.4	0.92	131.8

a) Nujol mull. b) Measured in dichloromethane. c) μ_I, nuclear magnetic moment; cited from Ref. 14. d) $\rho=A_{metal}/(\mu_I/I)$. e) One-electron reduced species of the Nb^V complex (**1**). f) Measured with **1**. g) ESR parameters cited from Ref. 1.

resemblance to that for **2** as depicted in **4** by referring to the X-ray crystallographic analysis of **1**.[2] On the basis of the same reasoning as mentioned for **2**, pyridine undergoes coordination with **1** at the same site that the oxo and acetato groups are placed even though the site becomes further sterically crowded. Such a profound effect and a strong affinity of niobium(V) for oxygen in part seem to be responsible for a weak coordination tendency of **1** toward pyridine, compared with other metalloporphyrins.[10]

Reduction and oxidation potentials for H_2TPP, **1**, and the corresponding molybdenum(V) complex, Mo(O)(TPP)(AcO) (**7**), are listed in Table 1. Table 2 summarizes the M=O stretching frequency for **1** and **7**, and spin Hamiltonian parameters for **7** and the one-electron reduced species of **1**. The one-electron reduced species of **1** shows ten intense lines over a wide range of magnetic field (1500—2000 G) due to hyperfine interaction with niobium nucleus (I=9/2). However, the superhyperfine structure due to four nitrogen nuclei was not detected for the present complex. Since both **7** and the one-electron reduced species of **1** provide ESR signals with remarkable intensity at room temperature, there is no excited d-orbital level placed close to the d-orbital of lowest energy for both species. Consequently, the second electron donated to the central metal atoms during the reductions, $Nb^{IV}\rightarrow Nb^{III}$ and $Mo^{V}\rightarrow Mo^{IV}$, must also be placed in the ground state orbital, which is then occupied with two electrons. The potential separation between first and second metal-reductions ($\Delta E_{1/2}$) for **1** is 0.16 V, while $\Delta E_{1/2}$ for **7** is 1.24 V since the corresponding processes for **7** are reductions of the Mo^{VI} and Mo^{V} species with reference to the number of d-electrons.

The acetato group seems to be released from the niobium(III) and molybdenum(IV) sites, as shown by structures **6** (Scheme 1) and **9** (Scheme 2) due to the reasons stated later, and both complexes may assume

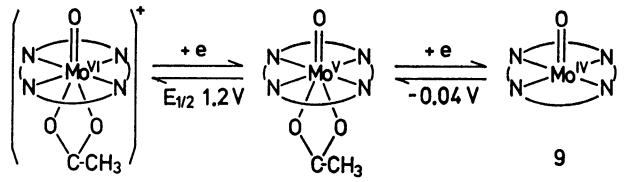

8 7 9

Scheme 2.

a similar coordination geometry consequently. On this basis, Racah's interelectronic repulsion parameters (B) for d^2 configuration[11] are cited for comparison; 682 and 602 cm^{-1} for Mo^{IV} and Nb^{III}, respectively. Such a small difference in Racah parameter, however, does not explain the large difference in $\Delta E_{1/2}$ stated above. The odd electron density at the metal nucleus is strictly reflected on hyperfine splitting constant A_{metal} for the same metal species. A ρ-value, which is proportional in general to the odd electron density at a metal nucleus, is given by $A_{metal}/(\mu_I/I)$ where μ_I and I stand for nuclear magnetic moment and nuclear spin, respectively. ρ-Values for the molybdenum(V) and niobium(IV) complexes of d^1 configuration listed in Table 2 are comparable to each other, and again do not explain the large difference in $\Delta E_{1/2}$.

In order to elucidate the origin of such potential difference, the change of coordination structures in the course of redox reactions needs to be taken into consideration as shown in Schemes 1 and 2. We reported previously the plausible structures at various metal oxidation states for **7**; **7**, **8**, and **9** in Scheme 2 for the Mo^{V}, Mo^{VI}, and Mo^{IV} species, respectively.[1] The molybdenum species in d^0 and d^1 configurations retain the acetato group while it seems liberated in d^2 configuration. The marked structural change assigned to **9** is reflected in its redox reaction rate. When the Mo^{IV}

species was electrolytically re-oxidized at 0 V *vs.* SCE under anaerobic conditions, it took about 12 h to return to the Mo^{V} state. On the other hand, when the Nb^{III} species in d^2 configuration was re-oxidized under anaerobic conditions, the ESR signal due to the Nb^{IV} species appeared in 1—2 min. However, even the Nb^{IV} species underwent electrolytic re-oxidation to the Nb^{V} state at 0 V *vs.* SCE under anaerobic conditions, the ESR signal due to the Nb^{IV} species still remained even after *ca.* 12 h of oxidation. On the basis of these kinetic results, structures **5** and **6** are reasonably assigned to the Nb^{IV} and Nb^{III} complexes, respectively.

By referring to equilibrium data for substitution reaction of Mo(O)(TPP)(MeO) with acetate and chloride ions[1] as well as the X-ray crystallographic analysis of Mo(O)(TPP)Cl,[12] the acetato group involved in **7** is coordinated to the molybdenum atom with some ionic character. Such an ionic character of the axial bond tends to stabilize the lowest d-orbital due to the effective positive charge localized on the molybdenum atom. An additional energy is required to cleave the axial bond in reduction process from **7** to **9**. Such a bond-cleavage effect is more pronounced for the reduction of Mo(O)(TPP)(MeO). Since the Mo–OMe bond has a significant covalent character as reported previously,[1] the lowest d-orbital would not be so much stabilized as in the case of **7**. Nevertheless, the reduction potential for Mo^{V}/Mo^{IV} was shifted toward cathodic direction by 0.7 V relative to the same potential for **7**.[1] Consequently, the axial bond cleavage seems predominantly to control the reduction potential for Mo^{V}/Mo^{IV}. A large $\Delta E_{1/2}$ value (1.24 V) for **7** is presumably due to such a bond cleavage effect, while a small $\Delta E_{1/2}$ value (0.16 V) confirms the **5**→**6** process which does not require the axial bond cleavage.

Both H_2TPP and **7** have comparable values of first and second potentials for the ligand reduction, the separation between the potentials being 0.33—0.4 V. This is consistent with the situation that the lowest d-orbital of **7** undergoes little interaction with ligand orbitals. On the other hand, not only the first ligand reduction potential for **1** is a little shifted toward cathodic direction, but also the separation between first and second reduction potentials is much larger than those for H_2TPP and the molybdenum complex. We conclude, therefore, that a considerable cathodic shift of the second ligand reduction potential in particular is attributed to an increase in π-electron density provided by delocalization of added two electrons in the ground state d-orbital of niobium through d-π interactions.

This work provides the first example for the two-electron reduction of the central metal atom to occur prior to the two-electron reduction of the macrocyclic ligand among metalloporphyrins involving second and third transition metals. Now, we are at the gate of research toward developments of stacked complex polymers by using a novel niobium(III) complex obtained in this work.

This work was supported in part by the Asahi Glass Foundation for Industrial Technology.

References

1) Y. Matsuda, S. Yamada, and Y. Murakami, *Inorg. Chem.*, in press.
2) C. Lecomte and J. Protas, *J. Chem. Soc., Chem. Commun.*, **1976**, 434.
3) J. F. Johnson and W. R. Scheidt, *J. Am. Chem. Soc.*, **99**, 294 (1977).
4) J. F. Johnson and W. R. Scheidt, *Inorg. Chem.*, **17**, 1280 (1978).
5) F. Endo, *Yakugaku Zasshi*, **79**, 595 (1959).
6) R. N. Adams, "Electrochemistry at Solid Electrodes," Marcel Dekker, New York, N. Y. (1969), pp. 143—162.
7) H. A. Benesi and J. H. Hildebrand, *J. Am. Chem. Soc.*, **71**, 2703 (1949).
8) K. M. Kadish, L. A. Bottomley, and J. S. Cheng, *J. Am. Chem. Soc.*, **100**, 2731 (1978).
9) J.-H. Fuhrhop and D. Mauzerall, *J. Am. Chem. Soc.*, **91**, 4174 (1969).
10) For example, see: F. A. Walker, *J. Am. Chem. Soc.*, **95**, 1150 (1973).
11) Racah's *B* parameters were evaluated from the energy separation between ^3F and ^3P states for free ions, Nb^{III} and Mo^{IV}. Term energies were cited from: C. E. Moore, "Atomic Energy Levels," Circular of the National Bureau of Standards 467, Washington, D. C. (1952, 1958), Vols. II and III.
12) H. Ledon and B. Mentzen, *Inorg. Chim. Acta*, **31**, L393 (1978).
13) A. Giraudeau, H. J. Callot, and M. Gross, *Inorg. Chem.*, **18**, 201 (1979).
14) Proceedings of the International Conference on Nuclear Moments and Nuclear Structure (1972); *Suppl. J. Phys. Soc. Jpn.*, **34** (1973).